

VLBI Observations of Water Masers in the Circumstellar Envelope of IRC+60169

Hiroshi SUDOU,¹ Toshihiro OMODAKA,² Hiroshi IMAI,^{3,4, *} Tetsuo SASAO,⁴
Hiroshi TAKABA,^{5,6} Masanori NISHIO,² Wataru HASEGAWA,² and Junichi NAKAJIMA⁶

¹ *Astronomical Institute, Graduate School of Science, Tohoku University, Aoba, Sendai 980-8578*
sudou@astr.tohoku.ac.jp

² *Faculty of Science, Kagoshima University, 1-21-30 Korimoto, Kagoshima 890-0065*

³ *Mizusawa Astrodynamics Observatory, National Astronomical Observatory, Mizusawa, Iwate 023-0861*

⁴ *VERA Project office, National Astronomical Observatory, 2-21-1 Osawa, Mitaka, Tokyo 181-8588*

⁵ *Faculty of Engineering, Gifu University, 1-1 Yanagido, Gifu 501-1193*

⁶ *Kashima Space Research Center, Communications Research Laboratory, Kashima, Ibaraki 314-0012*

(Received 2002 May 7; accepted 2002 August 3)

Abstract

Water masers around an AGB star, IRC+60169, were observed at four epochs using the Japanese VLBI networks. The distribution of the maser features is limited in a thick-shell region, which has inner and outer expansion velocities of 7 km s^{-1} and 14 km s^{-1} at radii of 25 mas and 120 mas, respectively. The distribution of the red-shifted features exhibits a ring-like structure, the diameter of which is 30 mas, and corresponds to the inner radius of the maser shell. This implies that dense gas around the star obscures red-shifted emission. Although a position–radial velocity diagram for the maser features is consistent with a spherical shell model, the relative proper motions do not indicate an expansion motion of the shell. A remarkable property has been found that is a possible periodic change of the alignment pattern of water maser spots.

Key words: masers — stars: circumstellar matter — stars: late-type — stars: individual (IRC+60169) — techniques: interferometric

1. Introduction

A low-mass star passes the Asymptotic Giant Branch (AGB) phase in the HR diagram, in which it undergoes heavy mass-loss processes. After the AGB phase, the star forms a planetary nebula (PN) by ionizing its circumstellar envelope (e.g., Kwok 1993). It has been stated that many young PNe exhibit a bipolar morphology or large deviation from spherical symmetry (e.g., Aaquist, Kwok 1991; Sahai et al. 1998). There still exists a missing link in the mass-loss history between AGB stars and central stars of PNe.

Most AGB stars show maser emission from water molecules (Reid, Moran 1981; Elitzner 1992). Masers have been used for probes of the mass-loss process in the circumstellar envelope of the AGB star. VLBI (Very Long Baseline Interferometry) observations have revealed that relatively young AGB stars (i.e., Mira variables and semi-regular variables) already exhibit bipolarity in their spherically expanding flows (e.g., Marvel 1997; Ishitsuka et al. 2001). On the other hand, for more evolved AGB stars (i.e., IRC/AFGL objects and OH/IR stars) and proto-PNe, little is known about the detailed mass-loss process by using the maser kinematics (cf., Marvel, Boboltz 1999;

Imai et al. 2002).

IRC+60169 has been classified as an IRC/AFGL object using the IRAS two-color diagram (van der Veen, Habing 1988; Takaba et al. 1994). It shows a clear double-peaked spectrum of water masers, which is a typical signature of IRC/AFGL objects and OH/IR stars. The shape of the spectrum exhibited a violent time variation. In 1977 the red-shifted component was stronger than the blue-shifted one, and in 1982 an intensity change between these components occurred (Engels et al. 1988). This fact is thought to be related to the temporary variation in the mass-loss flow.

We present the water-maser observations of IRC+60169 using Japanese VLBI networks in order to reveal the origin of the complicated time-variation in the intensity and distribution of the water masers and to investigate the kinematics of the circumstellar envelope by measuring the proper motions of the masers.

2. Observations

The water masers of IRC+60169 were observed using KNIFE (Kashima–Nobeyama InterFERometer; e.g., Miyoshi et al. 1993) on 1992 June 3 and J-Net (the Japanese domestic VLBI Network; e.g., Omodaka et al. 1994) on 1997 March 30, 1997 May 17, and 1998 April 4. The KNIFE system consists of two telescopes at

* Present address: Joint Institute for VLBI in Europe, Postbus 2, 7990 AA Dwingeloo, the Netherlands

Kashima and Nobeyama; its minimum fringe spacing is 14 mas. The J-Net system consists of four telescopes at Kashima, Nobeyama, Mizusawa, and Kagoshima; its minimum fringe spacing is 2 mas. The telescopes used for each observation are summarized in table 1. Since the quality of the data of the 2nd epoch taken at the Kagoshima telescope appeared to be poorer than those taken at the other telescopes, we flagged out the visibilities of baselines including this telescope. The received signals were recorded using the K-4 back-end system, which has 16 video channels with a band width of 2 MHz each (Kiuchi et al. 1997). Correlation processes have been carried out using the FX correlator at Mitaka (Chikada et al. 1991). Each video band was divided into 256 frequency channels, which corresponds to a velocity resolution of 0.11 km s^{-1} .

We used the NRAO AIPS package for fringe fitting and image synthesis. The extragalactic continuum source DA 193 was used as a calibrator of instrumental clock delays. Successive velocity channels containing the strong maser spots were used to calibrate the fringe rates. The same channels were also used as fringe-phase references for a self-calibration procedure. The absolute intensities at the 2nd, 3rd, and 4th epochs were not measured correctly because of a problem of a measurement of either system temperatures or conversion factors. The beam size of the KNIFE observation was about 14 mas with an almost circular shape, and those of the J-Net observations were 5.9×3.6 , 8.9×4.7 , and 6.3×3.7 [mas \times mas], at the 2nd, 3rd, and 4th epochs, respectively.

Maser emission is spatially resolved into some “maser features”, each of which consists of “maser spots” with almost similar positions and velocities (within ~ 5 mas and $\sim 1 \text{ km s}^{-1}$, respectively). The definitions of the words “feature” and “spot” are the same as those of Gwinn (1994) and Imai et al. (2000). The positions of the maser spots were estimated by using the AIPS task “JMFIT”, which is used for 2-dimensional Gaussian fits. We adopted the flux-weighted mean of the positions and the velocities of the maser spots as the position and velocity of the maser feature.

3. Results

Figure 1 is a spectral profile of water masers in IRC+60169 at the 1st epoch. They were detected over a range of between -10 km s^{-1} and -35 km s^{-1} . The intensity of the component near -33 km s^{-1} is the strongest in the spectrum. These characteristics are consistent with recent observations of this object (e.g., Colomer et al. 2000). Figure 2 shows the spatial distributions of the water-maser features at all four epochs. Tables 2–5 give parameters of the detected maser features at the individual epochs. We grouped them into two velocity components: blue-shifted ($\leq V_{\text{sys}}$) and red-shifted ($\geq V_{\text{sys}}$), where V_{sys} is the stellar systemic velocity, which is -24 km s^{-1} , given by the central velocity of the SiO-maser spectra (Engels et al. 1988). Hereafter, they are abbreviated as the B and R components, respectively. As shown in figures 2b, c, and d, the B component seems to be located in a limited region and

the R component appears to be distributed in a ring-like region around the B component.

Figure 3 shows a plot of the relative velocities of the maser features with respect to the stellar systemic velocity against the projected radial distance from a reference point. The reference point is the position of the brightest maser feature in each epoch. Assuming the standard thin-shell approximation, we obtained an inner shell radius R_{in} of ~ 25 mas (17 AU, assuming the distance of 690 pc; Loup et al. 1993) and an outer shell radius R_{out} of ~ 120 mas (83 AU). The expansion velocities at these radii are $\sim 7 \text{ km s}^{-1}$ and $\sim 14 \text{ km s}^{-1}$, respectively.

Comparing the positions and the velocities among the 2nd, 3rd, and 4th epochs, we identified eleven common maser features, which are labeled a, b, c, d, e, f, g, h, i, j, and k in tables 3–5. We did not use the data of the 1st epoch because of a too-long time span (~ 8 yr) to the next epoch. However, the maser distribution at the 1st epoch is not very different from those at the other epochs. The velocity of each maser feature was almost equal within 1 km s^{-1} among the epochs. Although each of two maser features, b and d, had two identifiable features between the 2nd and 3rd epochs, we traced the maser feature exhibiting more similar alignment patterns of maser spots. Features a, b, and j were detected at the 2nd, 3rd, and 4th epochs. Feature k was detected at the 2nd and 4th epochs. The other features were detected at the 2nd and 3rd epochs.

The proper motions of the maser features are shown in figure 5 and their parameters are summarized in table 6. The proper motions were measured relative to feature a, which was detected at the 2nd, 3rd, and 4th epochs. For features b and j, a weighted root-mean-square fit was carried out to obtain the proper motion during the three epochs. Figure 4 shows the fitting results for features b and j. The proper motions do not show a systematic motion that is expected from a spherically expanding shell model.

4. Discussion

4.1. Blocking Maser Emission by a Dense Circumstellar Envelope

In the case of Mira variables, red-shifted and blue-shifted components are always located in a small region, while intermediate components are always in a ring-like region. These components indicate radially and tangentially beamed masers, respectively (e.g., Lane et al. 1987). In order to obtain the averaged distribution among several years, we made a superposition of the distribution of the maser components of IRC+60169 with respect to the brightest component. Since the VLA observation of IRC+60169 reported by Colomer et al. (2000) showed the same morphology as ours, it was also added in this superposition. Figure 6a shows that the B components appeared to be in a limited region, such as blue-shifted components around Mira variables. On the other hand, in figure 6b, the R component appears to be in the ring-like region around the B component. This morphology

can be explained by a blocking effect proposed by Takaba et al. (1994): radially-beamed masers behind the blocking gas around the star are completely obscured, and all of the red-shifted masers widely distributed are the tangentially-beamed masers. Note that the R component, which is likely to be weakly beamed, is weaker than the B component. Engels et al. (1997) suggested an anti-correlation of intensities between the radial and tangential masers. This could be the reason why the intensity change between the B and the R components of IRC+60169 occurred in 1982.

The size of the obscuration was roughly estimated to be ~ 30 mas (21 AU), indicated from the diameter of the apparent absence of the R component. This value is in good agreement with the inner radius of the maser shell in figure 3 (~ 17 AU). The blocking material is the dense gas with a density of hydrogen molecules higher than 10^{10} cm $^{-3}$ and quenches water maser emission (Cooke, Elitzur 1985). This dense-gas region corresponds to the region where SiO-maser emission occurs, or the radio photosphere where H $^-$ and H $_2^+$ free-free absorption occurs (Reid, Menten 1997).

A blocking region has not been found in Mira variables. The radius of such a dense-gas region was found to be a few AU in Mira variables (e.g., Reid, Menten 1997). This value is too small to block water maser emission. However, the radius of the envelope is believed to increase with increasing luminosity or the mass-loss rate. Thus, the blocking region becomes larger when AGB stars evolve more. Although the luminosity has not been measured, the mass-loss rate of IRC+60169 was estimated to be an order of magnitude larger than that of typical Mira variables (Loup et al. 1993). This fact supports the idea that the blocking effect is significant in the envelope of IRC+60169

4.2. Environment of the Maser Shell in IRC+60169

The outer shell radius (83 AU) estimated from figure 3 is larger than that obtained by Colomer et al. (2000), because they were not able to detect the red-shifted component existing in the outer region of the shell. Although it is still smaller than a typical value for OH/IR stars or supergiants (~ 100 AU, e.g., Rosen et al. 1978; Yates, Cohen 1994), it is larger than that for Mira variables (~ 10 AU, e.g., Spencer et al. 1979; Bowers, Johnston 1994). One more important parameter of the maser shell is the logarithmic velocity gradient that describes the acceleration, $\epsilon = d(\ln V)/d(\ln R)$, where V is the expansion velocity and R is the radius of the shell. For the smaller value of ϵ , if the coherence path into the radial direction becomes longer, radial beaming occurs. In contrast, for a large value of ϵ , if the coherence path into the tangential direction becomes longer, tangential beaming occurs. Using the obtained parameters in the spherically expanding shell model for IRC+60169, we find $\epsilon \sim 0.4$. It is smaller than those obtained in Mira variables and semi-regular variables (Ishitsuka et al. 2001). This fact suggests that the radial masers are more dominant in IRC+60169 than Mira variables. Therefore, the radially-beamed, red-shifted masers are easy to suffer the blocking

effect.

4.3. Alignment Patterns of Maser Spots

It is stated that maser features exhibit a linear or curved maser-spots alignment in some supergiants (e.g., Richards et al. 1996, 1998) and some star-forming regions (e.g., Gwinn 1994; Torrelles et al. 2001), which are thought to be caused by shocks.

We focus our attention on the time variation of the maser-spots complex, including feature j and nearby features. Figure 7a shows the spatial distribution of maser spots consisting of individual features. The alignment pattern of the maser spots has changed between the 2nd and 3rd epochs, while at the 4th epoch, it appeared to be the same pattern as that at the 2nd epoch. The same tendency can be seen in the velocity distribution (figures 7b and c).

The alignment change is thought to be periodical and dominated by the pulsation of the star, because the time span between the 2nd and 4th epoch (360 d) is close to the IR variability period of IRC+60169 (440 ± 30 d, Lockwood 1985). This is explained by an analogy of the mode-switching effect proposed by Engels et al. (1997). The radius at which water masers occur could change according to the stellar brightness. If this hypothesis is correct, the proper motions of the maser features are a mixture of the bulk and pattern motions. This fact gives us difficulties in identifying the maser features and interpreting the proper motions.

4.4. Distance Measurement

Assuming an isotropic and random motion, we are able to estimate the distance to a star by applying the statistical parallax method (e.g., Genzel et al. 1981). Although the proper motion of the maser features in IRC+60169 might include the pattern motion of the maser cloud, we ignore this effect in this subsection. We have obtained the standard deviation of the Doppler velocities of 7.3 km s $^{-1}$ and those of the proper motions in the R.A. direction and the Dec. directions of 5.7 and 4.4 mas yr $^{-1}$, respectively. These values give distance values of 280 ± 50 pc and 360 ± 60 pc, respectively, taking into account the observational errors. On the other hand, the distance of 690 pc was suggested by assuming that the bolometric luminosity of IRC+60169 is $10^4 L_\odot$ (Loup et al. 1993). The underestimation of the distance could be caused by the blocking effect, because the radial velocity dispersion is underestimated. Assuming that the velocity distribution of the R component is the same as that of the B component, we obtain a velocity dispersion of 7.5 km s $^{-1}$, and the distance is estimated to be 290 and 370 pc, respectively. Further, adopting that the stellar systemic velocity is -23 km s $^{-1}$, suggested from CO observations (e.g., Lindqvist et al. 1988), we obtain a velocity dispersion of 8.4 km s $^{-1}$ and the distance is estimated to be 320 and 410 pc, respectively. Since these values are still smaller than the distance obtained by Loup et al. (1993), an intrinsic asymmetry of the velocity field of the envelope could be the reason for the underestimation of the distance.

5. Conclusions

In the present work, multi-epoch VLBI observations of the water masers in IRC+60169 were carried out. The main results from our data are described as follows: 1) The blocking effect is suggested by the ring-shaped distribution of the red-shifted maser features. The blocking size was estimated to be ~ 20 AU, which almost equals to the inner edge of the maser shell. This phenomena is believed to be seen only in evolved AGB stars. 2) The maser-shell size (~ 80 AU) suggests that IRC+60169 is more evolved than Mira variables. Although random motions are likely to dominate the kinematics of the envelope, radial acceleration also occurs in the maser shell. 3) We found that the alignment pattern of the maser spots seems to change periodically with the stellar pulsation. This implies that the spots pattern is stationary during a year, and that the environment in which masers occur moves to the radial direction. 4) Using the statistical parallax method, we obtained a weighted-mean distance to IRC+60169 of 310 ± 40 pc. This value is probably underestimated because of the blocking effect and/or the intrinsic asymmetrical velocity field.

Since we have measured only eleven proper motions, the kinematics of the circumstellar envelope in IRC+60169 is still unclear. Further systematic monitoring observations every few months will reveal the kinematics of the envelope, the distance, and the environment of the maser emitting region. In addition, SiO maser observations of IRC+60169 will be useful in revealing properties of the blocking gas, because it is considered to exist in it.

We would like to express our gratitude to each member of the Japanese VLBI networks for their support during observations, correlations, and data reduction. We also wish to thank an anonymous referee for useful comments. HI and HS were supported by the Grant-in-Aid for JSPS Fellows by Ministry of Education, Culture, Sports, Science and Technology.

References

- Aaquist, O. B., & Kwok, S. 1991, *ApJ*, 378, 599
 Bowers, P. F., & Johnston, K. J. 1994, *ApJS*, 92, 189
 Chikada, Y., Kawaguchi, N., Inoue, M., Morimoto, M., Kobayashi, H., Mattori, S., Nishimura, T., Hirabayashi, H., et al. 1991, in *Frontiers of VLBI*, ed H. Hirabayashi, M. Inoue, H. Kobayashi (Tokyo: Universal Academy Press), 79
 Colomer, F., Reid, M. J., Menten, K. M., & Bujarrabal, V. 2000, *A&A*, 355, 979
 Cooke, B., & Elitzur, M. 1985, *ApJ*, 295, 175
 Elitzur, M. 1992, *ARA&A*, 30, 75
 Engels, D., Schmid-Burgk, J., & Walmsley, C. M. 1988, *A&A*, 191, 283
 Engels, D., Winnberg, A., Walmsley, C. M. & Brand, J. 1997, *A&A*, 322, 291
 Genzel, R., Reid, M. J., Moran, J. M., & Downes, D. 1981, *ApJ*, 244, 884
 Gwinn, C. R. 1994, *ApJ*, 429, 253
 Imai, H., Kameya, O., Sasao, T., Miyoshi, M., Deguchi, S., Horiuchi, S., & Asaki, Y. 2000, *ApJ*, 538, 751
 Imai, H., Obara, K., Diamond, P. J., Omodaka, T., & Sasao T. 2002, *Nature*, 417, 829
 Ishitsuka, J. K., Imai, H., Omodaka, T., Ueno, M., Kameya, O., Sasao, T., Morimoto, M., Miyaji, T., Nakajima, J., & Watanabe, T. 2001, *PASJ*, 53, 1231
 Kiuchi, H., Amagai, J., Hama, S., & Imae, M. 1997, *PASJ*, 49, 699
 Kwok, S. 1993, *ARA&A*, 31, 63
 Lane, A. P., Johnston, K. J., Spencer, J. H., Bowers, P. F., & Diamond, P. J. 1987, *ApJ*, 323, 756
 Lindqvist, M., Nyman, L.-Å, Olofsson, H., & Winnberg, A. 1988, *A&A*, 205, L15
 Lockwood, G. W. 1985, *ApJS*, 58, 167
 Loup, C., Forveille, T., Omont, A., & Paul, J. F. 1993, *A&AS*, 99, 291
 Marvel, K. B. 1997, *PASP*, 109, 1286
 Marvel, K. B., & Boboltz, D. A. 1999, *AJ*, 118, 1791
 Miyoshi, M., KNIFE team 1993, in *Astrophysical Masers*, ed. A. W. Clegg, & G. E. Nedoluha (Heidelberg: Springer-Verlag), 441
 Omodaka, T., Morimoto, M., Kawaguchi, N., Miyaji, T., Yasuda, S., Suzuyama, T., Kitagawa, T., Miyazaki, T., et al. 1994, in *VLBI Technology, Progress and Future Observational Possibilities*, ed. T. Sasao, S. Manabe, O. Kameya, & M. Inoue (Tokyo: Terra Scientific Publishing Company), 191
 Reid, M. J., & Menten, K. M. 1997, *ApJ*, 476, 327
 Reid, M. J., & Moran, J. M. 1981, *ARA&A*, 19, 231
 Richards, A. M. S., Yates, J. A., & Cohen, R. J. 1996, *MNRAS*, 282, 665
 Richards, A. M. S., Yates, J. A., & Cohen, R. J. 1998, *MNRAS*, 299, 319
 Rosen, B. R., Moran, J. M., Reid, M. J., Walker, R. C., Burke, B. F., Johnston, K. J., & Spencer, J. H. 1978, *ApJ*, 222, 132
 Sahai, R., Trauger, J. T., Watson, A. M., Stapelfeldt, K. R., Hester, J. J., Burrows, C. J., Ballister, G. E., Clarke, J. T., et al. 1998, *ApJ*, 493, 301
 Spencer, J. H., Johnston, K. J., Moran, J. M., Reid, M. J., & Walker, R. C. 1979, *ApJ*, 230, 449
 Takaba, H., Ukita, N., Miyaji, T., & Miyoshi, M. 1994, *PASJ*, 46, 629
 Torrelles, J. M., Patel, N. A., Gómez, J. F., Ho, P. T. P., Rodriguez, L. F., Anglada, G., Garay, G., Greenhill, L., Curiel, S., & Cantó, J. 2001, *ApJ*, 560, 853
 van der Veen, W. E. C. J., & Habing, H. J. 1988, *A&A*, 194, 125
 Yates, J. A., & Cohen, R. J. 1994, *MNRAS*, 270, 958

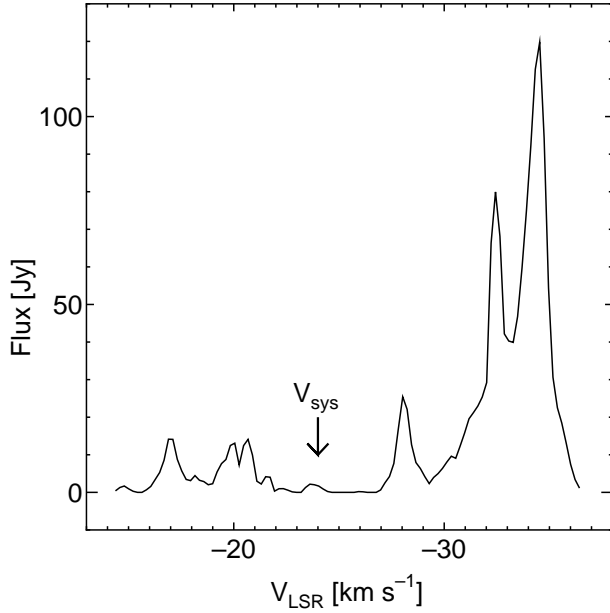


Fig. 1. Cross-correlated spectrum of the water maser emission of IRC+60169, obtained by the Kashima–Nobeyama baseline at the 1st epoch. V_{sys} is the stellar systemic velocity of IRC+60169.

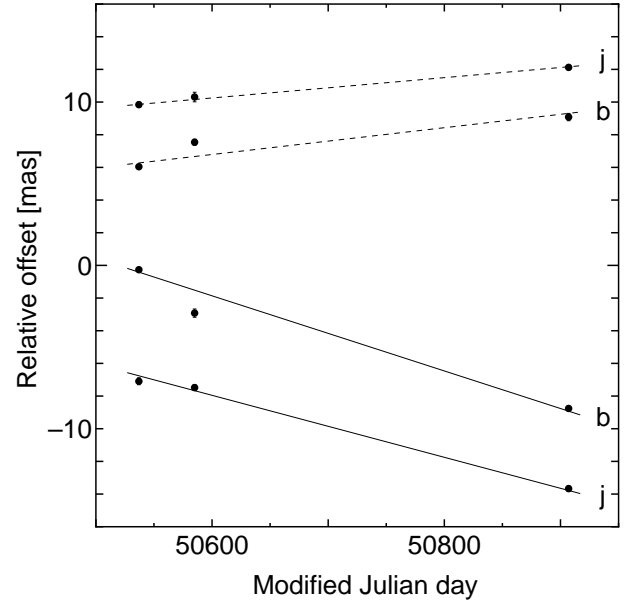


Fig. 4. Proper motions of the maser features b and j. The solid line indicates a least-squares fitted line assuming a constant velocity in the R.A. direction. The dotted line indicates that in the Dec. direction.

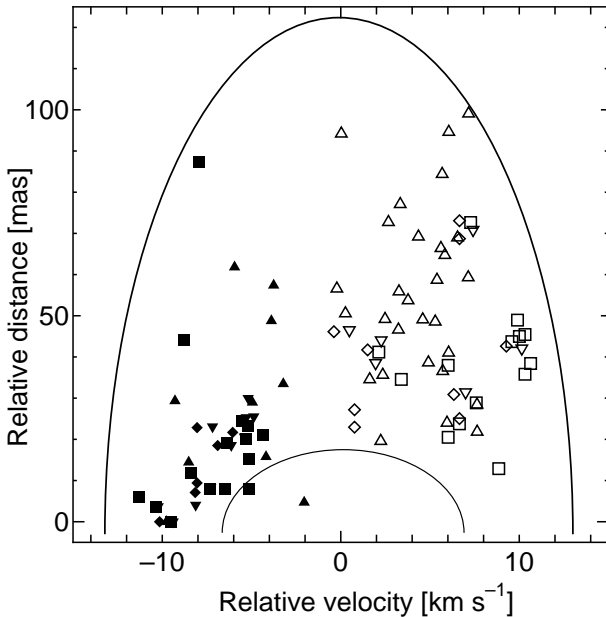


Fig. 3. Radial velocities of the maser features relative to the stellar velocity ($V_{\text{LSR}} = -24 \text{ km s}^{-1}$) plotted against the distances from the feature j. The filled and open marks indicate the B and R components, respectively. The triangles, inverse triangles, diamonds, and squares show the maser features at the 1st, 2nd, 3rd, and 4th epochs, respectively.

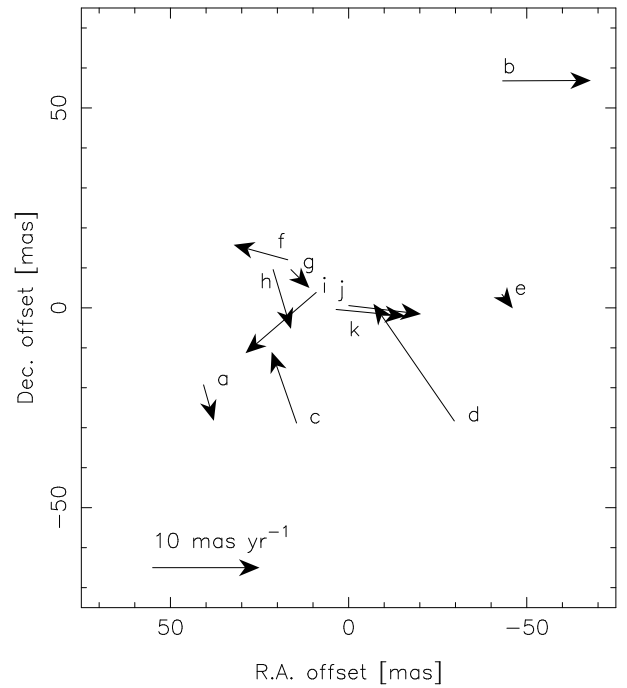


Fig. 5. Proper motions of the water maser features. We calculated the average of all of the proper-motion vectors and subtracted it from each proper-motion vector.

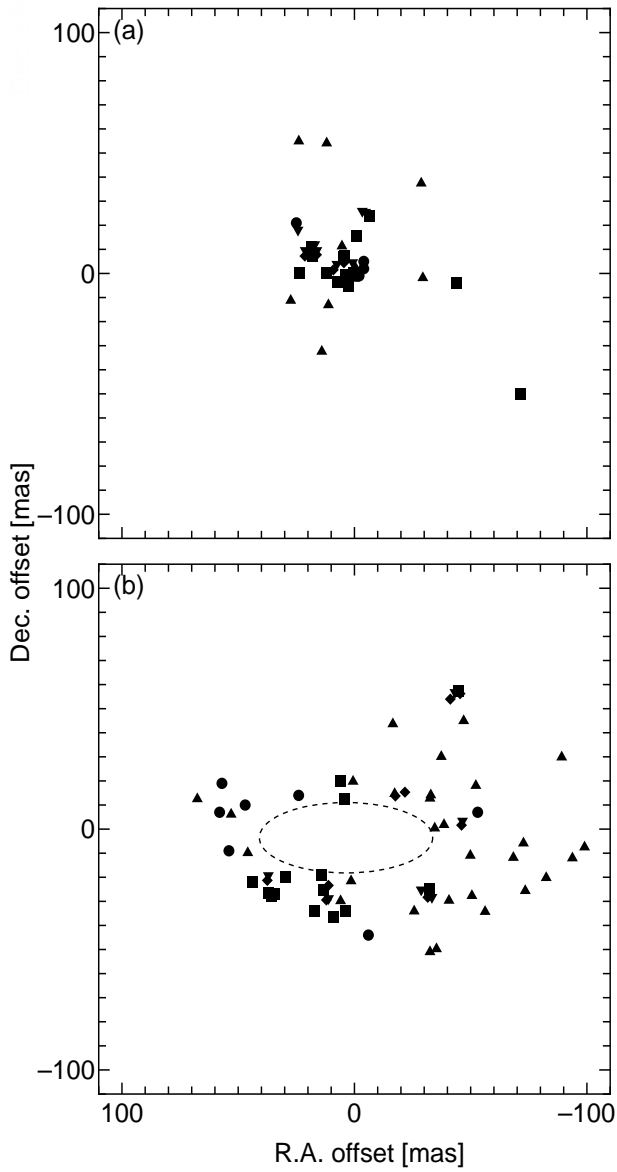


Fig. 6. Superposition of the maser feature distributions between 1990 and 1998 of (a) the B components and (b) the R components. The filled circles, triangles, inverse triangles, lozenges, and squares show the data of Colomer et al. (2000), the 1st, 2nd, 3rd, and 4th epochs of the present work, respectively. The dotted ellipse indicates the putative blocking region.

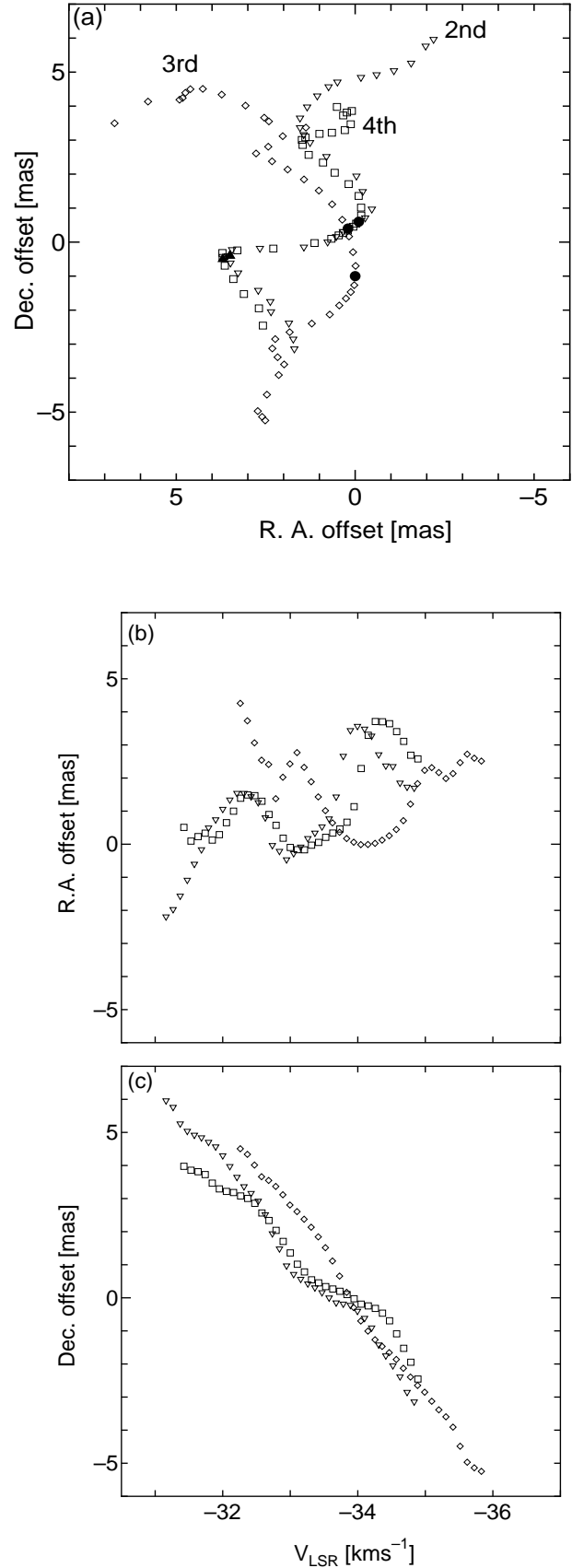


Fig. 7. Alignment change of the water maser spots in the features j and k, (a) R.A. vs. Dec., (b) V_{LSR} vs. R.A., and (c) V_{LSR} vs. Dec. The open inverse triangles, open diamonds, and open squares indicate the positions of the spots at the 2nd, 3rd, and 4th epochs, respectively. The filled circle and filled triangle show features j and k, respectively.

Table 1. Observing dates and participating telescopes.

Epoch	Date	Telescope*
1st	1992 June 3, 1992	O, N
2nd	1997 March 30	O, N, M, K
3rd	1997 May 17	O, N, M
4th	1998 April 4	O, M

* The keys to the telescopes are as follows.

O: 34-m telescope at Kashima.

N: 45-m telescope at Nobeyama.

M: 10-m telescope at Mizusawa.

K: 6-m telescope at Kagoshima.

Table 2. Parameters of the detected maser features at the 1st epoch (1992 June).

V_{LSR} [km s ⁻¹]	Δx^* [mas]	Error [mas]	Δy^\dagger [mas]	Error [mas]
-14.8	-34.1	0.5	-39.2	0.5
-16.9	-35.3	1.1	-49.6	0.2
-16.4	+6.0	0.9	-29.8	0.8
-16.4	+0.6	0.2	+19.8	0.3
-17.5	-68.4	0.8	-11.8	2.9
-16.8	-99.0	0.6	-7.5	0.7
-18.6	-32.5	0.6	-51.0	0.6
-18.0	-25.7	0.2	-34.1	0.2
-18.1	-17.3	0.5	+14.7	0.9
-18.0	-89.2	0.5	+29.9	1.3
-18.2	-56.2	0.2	-34.3	0.3
-18.3	-82.5	0.4	-20.2	0.3
-18.4	-47.0	0.7	+45.0	0.5
-18.3	-32.9	0.5	+14.1	0.4
-18.7	-16.5	0.3	+43.7	0.4
-19.1	-38.5	0.9	+1.8	2.1
-19.7	+67.6	0.8	+12.5	0.5
-19.4	-40.7	0.6	-29.6	0.5
-20.2	+53.0	3.3	+6.1	1.3
-20.8	+45.9	1.9	-9.9	0.2
-20.7	-73.5	0.2	-25.6	0.4
-21.3	-72.7	0.3	-5.9	0.3
-20.7	-52.2	0.4	+18.1	0.4
-21.5	-37.4	1.1	+30.1	0.2
-21.7	-32.5	0.1	+12.8	0.1
-21.8	+1.4	1.1	-21.6	0.9
-22.4	-34.5	0.6	+0.4	0.7
-23.7	-49.8	0.6	-11.0	0.4
-24.2	-50.5	0.5	-27.7	0.4
-24.0	-93.6	1.1	-12.0	0.5
-28.2	+11.2	0.3	-13.1	0.8
-26.1	-0.3	0.6	+2.7	0.5
-27.8	+12.0	0.5	+54.1	0.7
-27.9	-28.7	0.4	+37.4	0.7
-27.2	+14.1	0.9	-32.4	0.7
-29.0	+27.4	0.4	-11.2	0.6
-30.0	+23.9	1.2	+54.9	1.0
-33.8 [‡]	-0.1	0.9	-2.0	2.7
-32.5	+5.4	0.1	+11.4	0.2
-33.3	-29.4	0.4	-1.8	0.3

*Relative R.A. offset.

†Relative Dec. offset.

‡Maser feature containing the phase-reference spots.

Table 3. Same as table 2, but at the 2nd epoch (1997 March).

Feature	V_{LSR} [km s ⁻¹]	Δx^* [mas]	Error [mas]	Δy^\dagger [mas]	Error [mas]
a	-13.9	+37.0	0.2	-19.3	0.1
b	-16.6	-43.2	0.1	+56.8	0.1
c	-17.0	+11.1	0.1	-28.8	0.1
d	-21.7	-33.3	0.1	-28.4	0.1
...	-22.1	-28.7	0.3	-25.2	0.1
e	-23.5	-46.5	0.1	+3.37	0.3
f	-29.4	+17.1	0.1	+12.0	0.1
g	-30.1	+16.2	0.2	+9.6	0.2
...	-28.9	-3.4	0.3	+25.9	0.2
...	-29.2	+24.3	0.1	+18.0	0.1
...	-29.3	-4.8	0.2	+25.4	0.1
h	-31.2	+21.2	0.2	+9.6	0.2
i	-31.3	+7.5	0.1	+3.8	0.2
...	-32.1	+0.8	0.3	+4.5	0.2
j [‡]	-33.4	-0.1	0.2	+0.6	0.2
k	-34.2	+3.5	0.1	-0.4	0.2

*Relative R.A. offset.

†Relative Dec. offset.

‡See table 2.

Table 4. Same as table 2, but at the 3rd epoch (1997 May).

feature	V_{LSR} [km s ⁻¹]	Δx^* [mas]	Error [mas]	Δy^\dagger [mas]	Error [mas]
a	-14.7	+37.5	0.2	-21.3	0.2
b	-17.4	-45.4	0.3	+56.2	0.2
...	-17.4	-41.2	0.2	+54.0	0.2
...	-17.4	+11.2	0.2	-23.4	0.4
c	-17.7	+12.1	0.2	-29.4	0.4
d	-22.5	-31.5	0.2	-28.3	0.4
...	-23.2	-17.6	0.2	+13.8	0.2
...	-23.2	-21.7	0.2	+15.4	0.2
e	-24.4	-46.1	0.2	+1.6	0.2
f	-30.1	+18.3	0.2	+10.7	0.3
g	-30.9	+16.3	0.4	+7.8	0.2
h	-32.1	+21.3	0.2	+7.2	0.2
i	-32.1	+9.1	0.2	+1.5	0.2
...	-32.2	+4.5	0.3	+4.5	0.2
j [‡]	-34.2	+0.0	0.2	-1.0	0.3

*Relative R.A. offset.

†Relative Dec. offset.

‡See table 2.

Table 5. Same as table 2, but at the 4th epoch (1998 April).

Feature	V_{LSR} [km s ⁻¹]	Δx^* [mas]	Error [mas]	Δy^\dagger [mas]	Error [mas]
...	-13.4	+17.1	0.2	-34.2	0.1
...	-13.7	+36.9	0.4	-26.5	0.4
...	-14.0	+35.5	0.3	-27.6	0.1
...	-14.4	+34.3	0.2	-27.0	0.4
...	-13.7	+29.6	0.1	-20.1	0.1
a	-14.1	+43.9	0.1	-21.8	0.1
...	-15.2	+4.1	0.1	+12.6	0.2
...	-16.4	+13.3	0.1	-25.4	0.2
b	-16.7	-44.9	0.1	57.3	0.2
...	-17.4	+14.1	0.1	-18.9	0.1
...	-18.0	+5.8	0.2	+20.1	0.2
...	-18.0	+9.1	0.2	-36.6	0.1
...	-20.6	+3.9	0.1	-34.0	0.1
...	-21.9	-32.3	0.2	-25.0	0.2
...	-28.4	+18.6	0.1	+10.8	0.2
...	-29.1	+4.5	0.1	+7.1	0.2
...	-29.1	-0.9	0.2	+15.5	0.1
...	-29.2	+23.5	0.2	+0.1	0.1
...	-29.3	+18.3	0.1	+8.9	0.1
...	-29.5	-6.4	0.1	+24.0	0.1
...	-30.4	+17.9	0.3	+7.4	0.1
...	-30.5	+4.7	0.2	+6.9	0.2
...	-31.3	+7.2	0.2	-3.5	0.2
...	-32.0	-71.3	0.1	-50.0	0.1
...	-32.8	-43.8	0.2	-3.9	0.1
...	-32.4	+12.1	0.1	+0.2	0.3
j [‡]	-33.5	+0.2	0.2	+0.4	0.1
k	-34.4	+3.7	0.1	-0.5	0.2
...	-35.3	+2.5	0.1	-5.2	0.2

*Relative R.A. offset.

†Relative Dec. offset.

‡See table 2.

Table 6. Parameters of the proper motions of the maser features in IRC+60169.

Feature	μ_x^* [mas yr ⁻¹]	Error [mas yr ⁻¹]	μ_y^\dagger [mas yr ⁻¹]	Error [mas yr ⁻¹]
a	+0.3	0.5	-3.0	0.3
b	-8.2	0.2	+0.0	0.4
c	+3.5	0.4	+5.9	0.6
d	+8.8	0.3	+9.3	0.6
e	+0.1	0.3	-1.2	0.5
f	+5.1	0.3	+1.2	0.4
g	-1.7	0.6	-1.5	0.4
h	-1.7	0.4	-4.9	0.4
i	+7.1	0.3	-5.1	0.3
j	-6.8	0.3	-0.7	0.3
k	-6.5	0.2	-0.6	0.4

*Motions in the R.A. direction.

†Motions in the Dec. direction.

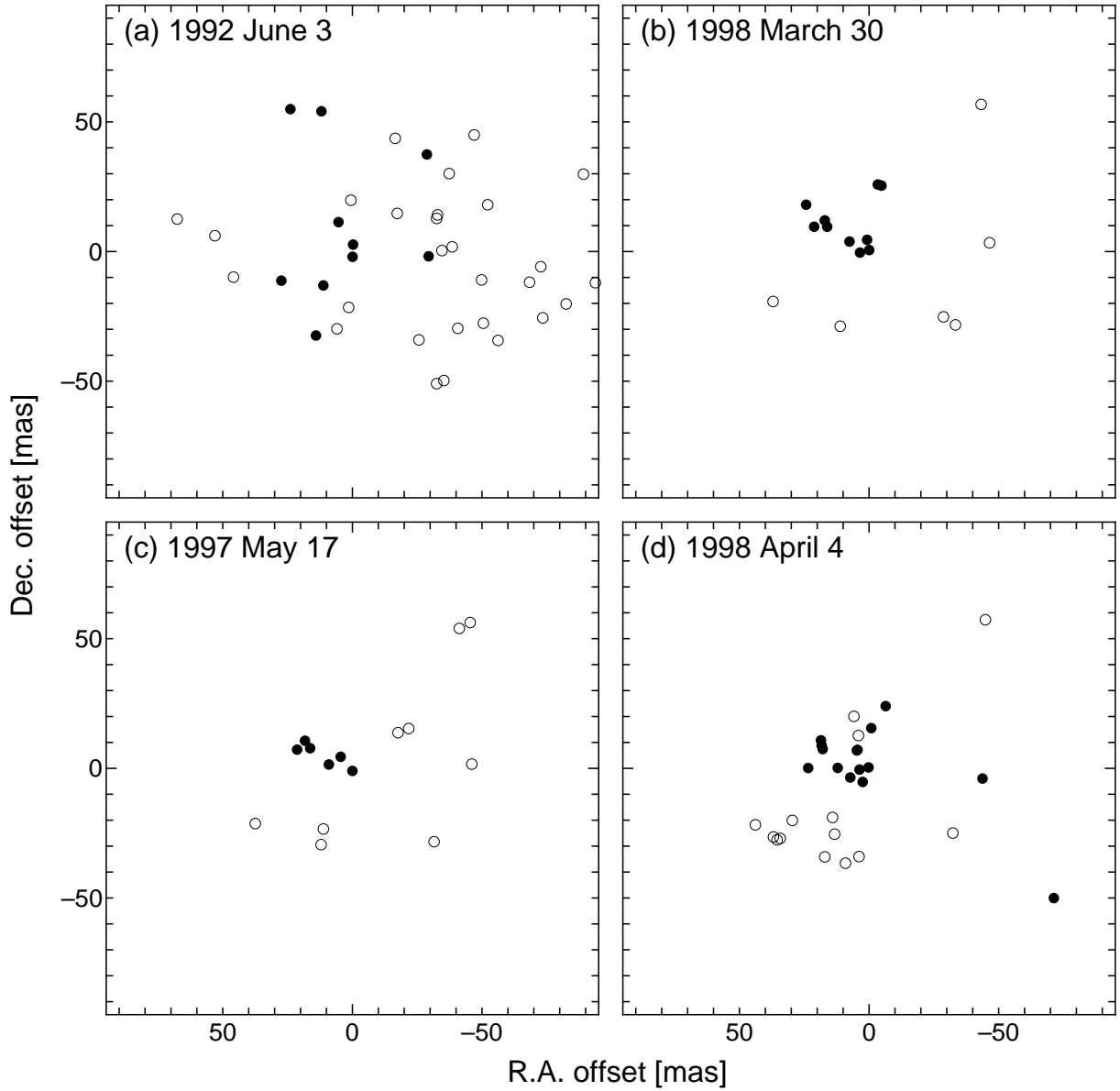


Fig. 2. Distributions of the water maser features of IRC+60169 on (a) 1992 June 3, (b) 1997 March 30, (c) 1997 May 7, and (d) 1998 April 4. The open and filled circles indicate the maser features of the B and R components, respectively.